Volume 17, No 1 | International Journal of Radiation Research, January 2019

Designing a shield to reduce radiation dose during mammography: Dosimetric evaluation

D.Y. Lee[1] and J.S. Lee[2*]

[1]Department of Radiation Oncology, Dongnam Institute of Radiological & Medical Sciences Cancer Center, 40, Jwadong-gil, Busan, Republic of Korea
[2]Department of Radiology, Inje University Haeundae Paik Hospital, 875, Haeundae-ro, Haeundae-gu, Busan, Republic of Korea

► ***Original article***

Corresponding authors:
Jin Soo Lee, PhD.,
Fax: *+82 51 797 0382*
E-mail:
sonojinsoo@naver.com

Revised: March 2018
Accepted: June 2018

Int. J. Radiat. Res., January 2019; 17(1): 127-135

DOI: 10.18869/acadpub.ijrr.17.1.127

ABSTRACT

Background: This paper presents a method to reduce radiation exposure during mammography by analysing the doses to ipsilateral and contralateral breasts and to adjacent organs by evaluating material-dependent shielding performance. ***Materials and Methods***: Six target-filter combinations (Mo-Mo, Mo-Rh, Rh-Rh, Rh -Mo, W-Mo, W-Rh) were tested by measuring the doses delivered to the breasts and adjacent organs, with the contralateral (opposite side) breast shielded. The shield was designed to have a simple (ㄱ , ㄷ) shape for ease of use in actual clinical settings, using lead, copper, bismuth, and barium sulphate (BaSO4) as materials for shield configuration. ***Results:*** The dosimetric data revealed that the highest absorbed dose was exhibited by the target filter combination of Rh/Rh, followed by W/Rh, W/Mo, Rh/Mo, Mo/Rh, and Mo/Mo. Additionally, the radiation dose was reduced by 54–55%, with the average absorbed dose on the contralateral breast reduced from 0.655 to 0.359 mGy. All four shielding materials used in the experiments were analysed for the shielding effect. ***Conclusion:*** This Using a shield during screening mammography would alleviate concerns about the mammography-induced risk of breast cancer and secondary effects.

Keywords: *Mammography, Simulation, Shielding material, Contralateral dose*

INTRODUCTION

Globally, breast cancer is the second most frequently diagnosed cancer in women, and the leading cause of cancer death in women [1-2]. Efficient ways to reduce the incidence of breast cancer include minimizing exposure to the risk factors for breast cancer and identifying a high-risk group to provide appropriate preventive measures. Most important tools for early detection of breast cancer are breast self-examination technique and screening mammography [3]. There is a general consensus that these methods play pivotal roles in the early detection and treatment of breast cancer [4]. With the increasing incidence of breast cancer, the frequency of breast screening has been increasing [5]. Breast screening contributes to substantially reducing breast cancer mortality rate [1]. Mammography is the most efficient and accurate method for early detection of breast cancer [6-7]. In particular, introduction of digital mammography has contributed to overcoming the technical and structural limitations of the conventional film-screen mammography. Digital mammography has technical advantages over film-screen mammography, such as smaller X-ray absorption difference (contrast) between lesions and mammary gland tissue owing to its high X-ray absorption rate, enhanced imaging of microcalcifications, and maximum convenience due to automatic exposure condition configuration adjusted to breast thickness [8]. With the growing frequency of mammography,

focused efforts have been directed at minimizing the side effects of radiation exposure. Concerns about potential risk of cancer from mammography have constantly been raised, especially because mammary gland tissue is highly radiation-sensitive [9-12]. While mammography is generally performed on both breasts in the craniocaudal (CC) and mediolateral oblique (MLO) views, special views, such as magnification or spot compression views, can be additionally obtained in case of suspected diseases or lesions [13]. Therefore, at least 2–3 images are acquired each breast, which can lead to an increase in the dose directly delivered to the breast being imaged and the scattered radiation to adjacent organs. In addition, because the extent to which the dose to the contralateral breast increases is not negligible, the exposure dose should be dosimetrically monitored during mammography and the contralateral breast should be shielded from the scatter dose. This paper presents a method to reduce radiation exposure during mammography by analysing the doses to ipsilateral and contralateral breasts and to adjacent organs by evaluating material-dependent shielding performance. Simulations were performed with the Monte Carlo N. Particle Extended (MCNPX) software package.

MATERIALS AND METHODS

Quantitative evaluation of radiation exposure of the human body may be obtained most reliably from experiments on the human body. This being impossible, however, we performed phantom-based radiation simulations in a virtual space using MCNPX (Ver.2.5.0). After modelling mammographic equipment and anthropomorphic computational phantoms for radiation using the MCNP code, experiments were carried out in two categories. First, the properties of the generated photons were evaluated by analysing the photon spectrum for each target-filter combination. Second, radiation exposure of adjacent organs during mammography was dosimetrically evaluated depending on the shielding or non-shielding of the contralateral breast, thereby varying the shielding material.

1. Mammography equipment

Figure 1 shows the mammography equipment setting simulated with the MCNP code.

Simulation was performed in the order of the target, X-ray tube, permanent filter, and additional filter. Targets were designed to have a gradient of 9° and three different materials were chosen: molybdenum (atomic number: 42, density: 10.28 g/cm^3), rhodium (atomic number: 45, density: 12.41 g/cm^3), tungsten (atomic number: 74, density: 19.25 g/cm^3) [14]. The permanent filter was configured to have a thickness of 0.63 mm using beryllium (atomic number: 4, density: 1.85 g/cm^3) as the material. The additional filter was configured to have a thickness of 0.25 μm using molybdenum and rhodium as materials. Six different target-filter (additional filter) combinations were configured: Mo-Mo, Mo-Rh, Rh-Rh, Rh-Mo, W-Mo, and W-Rh. The selected materials and thicknesses of individual parts and target-filter combinations are the ones most commonly used in clinical settings [15].

Computational breast phantom

We chose phantoms for computational radiation dosimetry from the UF-revised phantom series developed by University of Florida, USA, which are age-specific—from new-borns (0 year) to adults (30 years)—and gender-specific [16]. The body composition and physical properties were simulated on the basis of International Commission on Radiation Protection (ICRP) 89[17] and International Commission on Radiation Units and Measurements (ICRU) 46[18]. Apart from this, the adipose and glandular breast tissues composing the breast phantom were configured to have proportions of 50% each, as presented in ICRU 44 [19]. Table 1 outlines the physical properties of the adipose and glandular tissues of the breast phantom.

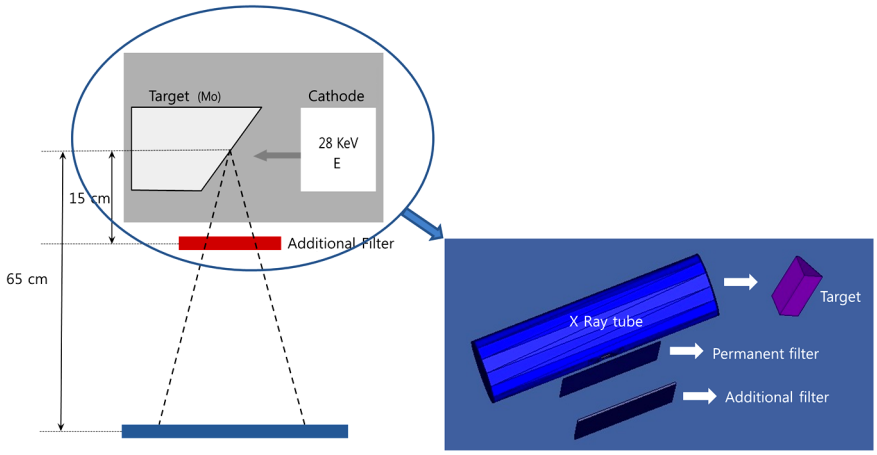

Figure 1. Mammography equipment simulated with the MCNP code.

Table 1. Composition of the breast phantom.

Element	Adipose	Mammary gland
H	11.4	10.6
C	59.8	33.2
N	0.7	3.0
O	27.8	52.7
Na	0.1	0.1
Cl	0.1	0.1
S	0.1	0.2
P		0.1
Density (g/cm^3)	0.95	1.02

Geometric shapes of ellipse, cone, plane, and cylinder are usually used to configure the surface morphology of mathematical (computational) phantoms for radiation dosimetry simulated in a three-dimensional virtual space. The structures thus expressed can be defined by equations; for example, the shapes of the breast, lung and heart, key organs of the phantoms used in this study were expressed with ellipsoid, paraboloid, and hyperboloid, respectively. The configuration can be defined by Eq. (1).

$$A(x-\bar{x})^2 + B(y-\bar{y})^2 + C(z-\bar{z})^2 + 2D(x-\bar{x}) + 2E(y-\bar{y}) + 2F(z-\bar{z}) + G = 0 \quad (1)$$

where the x-, y-, and z-axes represent the right-left, front-rear, and foot-head directions, respectively, of the phantom body. The unit of measure on the coordinate plane is centimetre.

Photon spectrum measurement

Photon spectrum analyses were performed on the aforementioned six target-filter combinations using the X-ray tube simulated earlier. We measured the number of photons generated per electron (e) at a tube voltage of 28 kVp, using tally F5. The photon number/cm^2/e was measured by placing a virtual circular detector with a diameter of 5 cm at a distance of 65 cm point from the target centre. The spectrum measurement interval was set at 1 eV. The margin of error was narrowed down to 3% or lower by setting the nps value, which represents the number of replicates, at 10^8 in order to improve the accuracy of experimental results.

Dosimetric evaluation of the breasts and adjacent organs

We measured the doses delivered to the breasts and adjacent organs of the UF-revised phantoms, with the contralateral breast shielded, and evaluated the results obtained

from the six target-filter combinations at a tube voltage of 28 kVp. As shown in figure 2, the shield was simulated to have a simple structure of ¬ , ⌐ shape designed for convenient use in clinical settings. Lead, copper, bismuth, and barium sulphate (BaSO4) were used as materials for shield configuration. The thickness of the shield was set at 1 mm for all the materials, based on the finding of a study that a 50 kVp photon beam is attenuated by 99.9% at 0.5 mm lead equivalent [20]. Organ dosimetry was performed on the breasts, lungs, and heart ipsilaterally or contralaterally. Tally F6 was used to obtain the dosimetric values in MeV/g, which was then converted into absorbed dose (mGy). The reliability of the simulation results was ensured by keeping the error below 3% and the nps, which denotes the number of simulation trials, was 10^8.

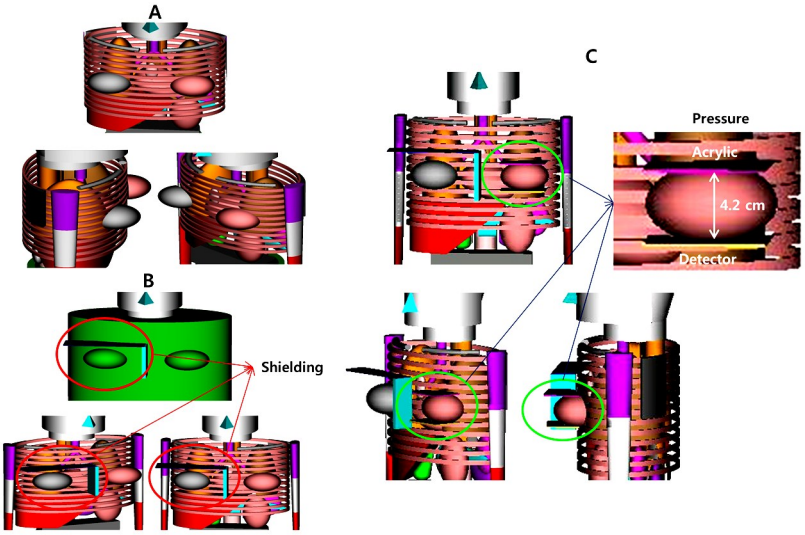

Figure 2. Computational phantoms used in the simulation. **A)** Breast phantom used in the simulation, **B)** shielding the contralateral breast, **C)** pressure on the ipsilateral breast.

RESULTS

Photon Spectrum Analysis

The graphs in figure 3 present the photon spectra measured on each of the target-filter combinations. In order to determine the effect of the additional filter, the photon spectra of the configurations with and without the additional filter were compared and analysed. Table 2 presents the characteristic and average energies as well as the photon fluxes.

The dosimetric results reveal that photon flux ranged from 1.91E-07 to 1.46E-06 photons/cm^2/e, with tungsten (W) showing the highest count, followed by molybdenum (Mo) and rhodium (Rh). Mo exhibited the highest average energy, followed by Rh and W, tending upwards owing to the additional filter. The usage of Mo and Rh as the additional filters resulted in an increase in the average energy by about 5 and 6.5 keV, respectively. As regards the characteristic ray, characteristic energies measured on the three targets were as follows: 17.5, 19.6, and 20.0 keV on Mo; 20.2, 22.7, and 23.2 keV on Rh; and 8.9, 17.5, and 20.2 keV on W.

Absorbed dose to the contralateral breast

Figure 4 shows the different absorbed doses to the contralateral breast depending on whether it is shielded or unshielded.

First, when the left breast was imaged, the average absorbed dose to the unshielded right breast was analysed to be 6.55E-01 mGy, accounting for ~43.7% of the left breast, which fell to 3.58E-01 mGy (23.9%) when shielded. The average radiation dose was calculated at ~54.6%.

Second, when the right breast was imaged, the average absorbed dose to the unshielded left breast was analysed to be 6.53E-01 mGy,

accounting for ~43.6% of the right breast, which fell to 3.60E-01 mGy (24.0%) when shielded. The average radiation dose was calculated at ~55.1%.

Third, the material-dependent differences in the radiation dose were found to be negligible, with the average absorbed dose ranging between 3.52E-01 mGy and 3.67E-01 mGy.

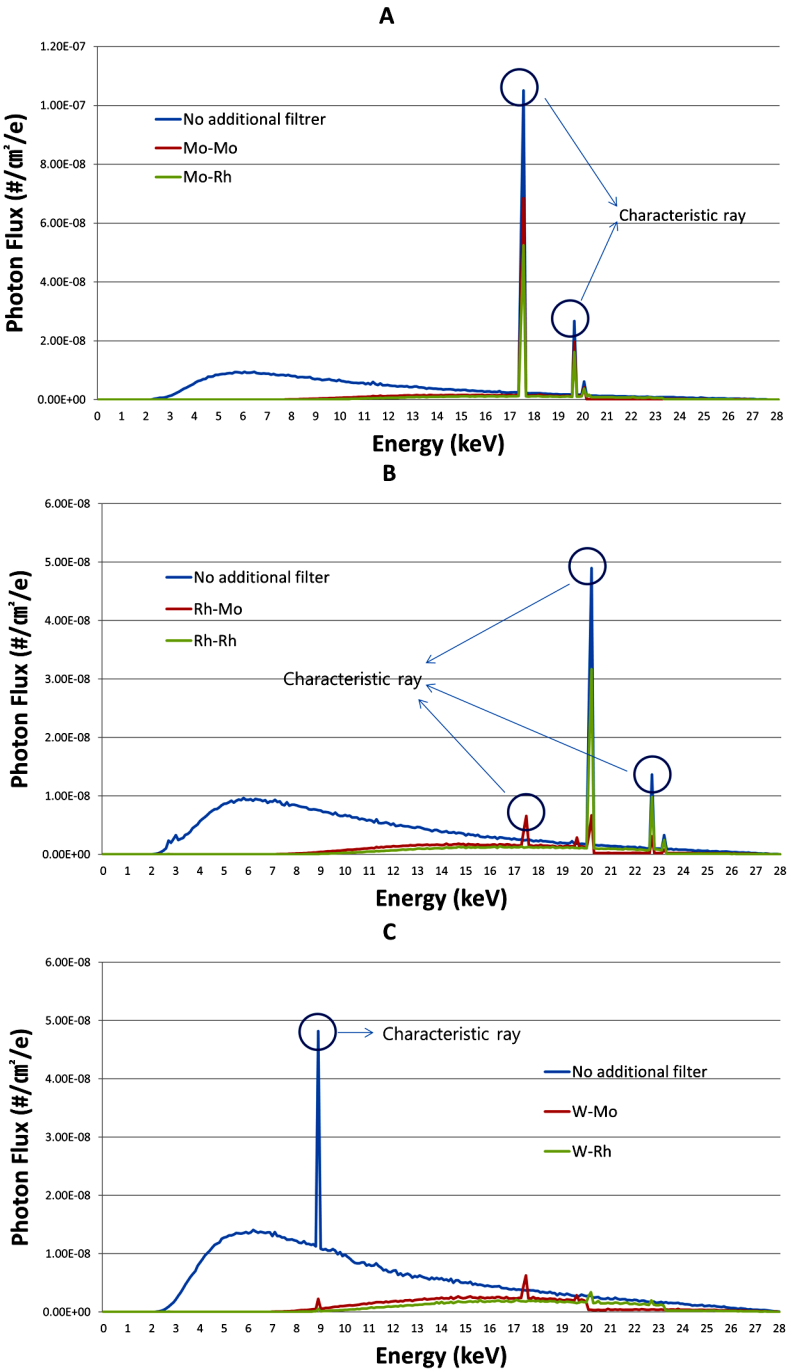

Figure 3. Spectra of photons measured in MCNPX. **A)** Photon spectrum calculated when the target material is molybdenum, **B)** Photon spectrum calculated when the target material is rhodium, **C)** Photon spectrum calculated when the target material is tungsten.

Table 2. Flux, characteristic, and average energy of photon measured in MCNPX.

Target / Additional filter	Flux (Photon number/cm^2/e)	Characteristics energy (keV)	Average energy(keV)
Mo	1.12E-06	17.5, 19.6, 20.0	11.6
Mo / Mo	2.82E-07	17.5, 19.6, 20.0	16.5
Mo / Rh	2.21E-07	17.5, 19.6, 20.0	17.4
Rh	1.06E-06	20.2, 22.7, 23.2	11.3
Rh / Mo	1.91E-07	20.2, 22.7, 23.2	16.0
Rh / Rh	1.92E-07	20.2, 22.7, 23.2	18.2
W	1.46E-06	8.9	10.6
W / Mo	2.57E-07	8.9, 17.5	15.8
W / Rh	2.05E-07		17.4

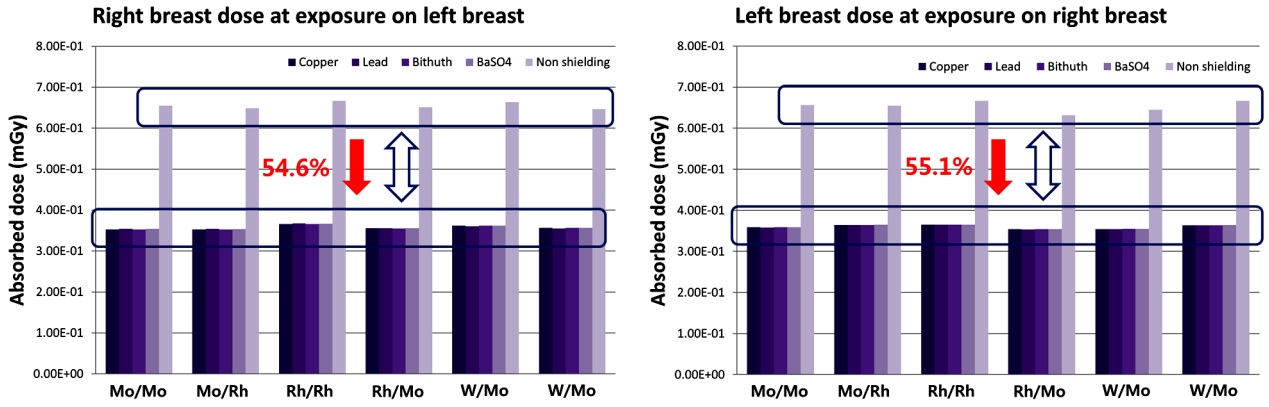

Figure 4. Absorbed dose to the contralateral breast.

Absorbed dose to adjacent organs

Tables 3 and 4 present the absorbed doses to the organs (lungs and heart) adjacent to the ipsilateral breast under mammographic examination. The absorbed dose was measured under the shielded or unshielded conditions and when the contralateral breast is shielded for six target-filter combinations on left and right organs, thereby varying the shield configuration among four materials.

First, analyses of the measurements under the unshielded conditions yielded the following results: The highest average absorbed dose was exhibited by the ipsilateral lung (1.37E-02 mGy), followed by the contralateral lung (1.07E-02 mGy) and heart (7.85E-03 mGy), accounting for 0.91, 0.71, and 0.52%, respectively, of the dose absorbed by the breast being imaged.

Second, analyses of the measurements under the shielded conditions yielded the following results: The highest average absorbed dose was exhibited by the ipsilateral lung (1.39E-02 mGy), followed by the contralateral lung (1.39E-02 mGy) and heart (5.61E-03 mGy), accounting for 0.92, 0.68, and 0.37%, respectively, of the dose absorbed by the breast being imaged.

From the analysis results, it can be confirmed that shielding tends to increase the absorbed dose to the ipsilateral lung while decreasing the absorbed dose to the contralateral lung and heart.

Third, the highest absorbed dose was exhibited by the Rh/Rh target-filter combination, followed by W/Rh, W/Mo, Rh/Mo, Mo/Rh, and Mo/Mo.

Table 3. Absorbed dose to the adjacent organs when the left breast was imaged.

Organ	Shielded	Target–filter combination					
		Mo/Mo	Mo/Rh	Rh/Rh	Rh/Mo	W/Mo	W/Rh
Lt. Lung	Non-shielding	1.02E-02	1.19E-02	1.75E-02	1.29E-02	1.41E-02	1.65E-02
	Copper	1.01E-02	1.17E-02	1.80E-02	1.31E-02	1.38E-02	1.73E-02
	Lead	1.02E-02	1.19E-02	1.81E-02	1.33E-02	1.39E-02	1.73E-02
	Bithmuth	1.01E-02	1.17E-02	1.80E-02	1.31E-02	1.38E-02	1.73E-02
	BaSO4	1.01E-02	1.18E-02	1.80E-02	1.32E-02	1.38E-02	1.73E-02
Rt. Lung	Non-shielding	8.12E-03	9.55E-03	1.42E-02	9.82E-03	1.02E-02	1.46E-02
	Copper	7.44E-03	8.98E-03	1.36E-02	9.22E-03	9.29E-03	1.35E-02
	Lead	7.41E-03	9.01E-03	1.35E-02	9.21E-03	9.35E-03	1.36E-02
	Bithmuth	7.40E-03	9.01E-03	1.36E-02	9.22E-03	9.31E-03	1.35E-02
	BaSO4	7.40E-03	9.00E-03	1.36E-02	9.20E-03	9.34E-03	1.36E-02
Heart	Non-shielding	5.46E-03	6.54E-03	1.08E-02	7.84E-03	7.66E-03	1.07E-02
	Copper	3.79E-03	5.10E-03	7.82E-03	5.90E-03	4.93E-03	7.53E-03
	Lead	3.83E-03	5.17E-03	7.81E-03	5.96E-03	5.01E-03	7.59E-03
	Bithmuth	3.79E-03	5.12E-03	7.88E-03	5.90E-03	4.93E-03	7.52E-03
	BaSO4	3.81E-03	5.13E-03	7.84E-03	5.94E-03	4.96E-03	7.57E-03

Table 4. Absorbed dose to the adjacent organs when the right breast was imaged.

Organ	Shielded	Target–filter combination					
		Mo/Mo	Mo/Rh	Rh/Rh	Rh/Mo	W/Mo	W/Rh
Lt. Lung	Non-shielding	6.77E-03	9.41E-03	1.45E-02	9.06E-03	9.39E-03	1.25E-02
	Copper	6.59E-03	8.94E-03	1.44E-02	9.24E-03	9.14E-03	1.22E-02
	Lead	6.53E-03	8.97E-03	1.44E-02	9.21E-03	9.13E-03	1.22E-02
	Bithmuth	6.60E-03	8.95E-03	1.44E-02	9.25E-03	9.16E-03	1.22E-02
	BaSO4	6.56E-03	8.97E-03	1.44E-02	9.19E-03	9.14E-03	1.22E-02
Rt. Lung	Non-shielding	8.93E-03	1.19E-02	1.85E-02	1.23E-02	1.26E-02	1.71E-02
	Copper	9.05E-03	1.17E-02	1.88E-02	1.25E-02	1.28E-02	1.71E-02
	Lead	9.03E-03	1.18E-02	1.87E-02	1.24E-02	1.28E-02	1.71E-02
	Bithmuth	9.06E-03	1.17E-02	1.87E-02	1.25E-02	1.28E-02	1.71E-02
	BaSO4	9.08E-03	1.18E-02	1.88E-02	1.25E-02	1.29E-02	1.72E-02
Heart	Non-shielding	6.67E-03	6.68E-03	1.01E-02	6.60E-03	5.76E-03	9.33E-03
	Copper	4.19E-03	4.31E-03	7.87E-03	4.50E-03	4.62E-03	6.65E-03
	Lead	4.13E-03	4.28E-03	7.89E-03	4.56E-03	4.61E-03	6.62E-03
	Bithmuth	4.19E-03	4.31E-03	7.89E-03	4.50E-03	4.48E-03	6.65E-03
	BaSO4	4.18E-03	4.31E-03	7.88E-03	4.53E-03	4.49E-03	6.63E-03

DISCUSSION

The internationally recommended maximum average glandular dose to the breast in mammography is 1.5–2 mGy. However, even in cases where the breast being imaged is exposed to less than 3 mGy, most mammographic exams are conducted in a series of mammograms in CC and MLO views, and additional mammograms in different views further increase the overall exposure dose [13]. Against this background, simulations were performed in this study in an effort to minimize unnecessary irradiation by shielding the contralateral breast during screening mammography.

First, photon spectrum analysis was performed to establish reliability of the X-ray tube modelled for simulation. A previous study [21] measured the characteristic energies of molybdenum targets as 17.5 keV and 19.5 keV. In the present work, molybdenum showed similar tendencies with obtained values of 17.5

keV, 19.6 keV, and 20.0 keV. Furthermore, the photon spectra from the previous studies [22-23] were relatively linear for molybdenum and rhodium, and continuous for tungsten, because their filters absorb the low-energy part. In this study, the absorption of the low-energy part is remarkable when the filter is used, and thus, the shape of the spectrum obtained is similar.

Second, the absorbed dose to the unshielded contralateral breast made up 43.5–43.6% of the dose directly delivered to the breast being imaged. When shielded, the dose decreased to 23.9–24%. By comparing the measurements with and without the shield, the radiation dose was calculated at ~54–55%. This relatively low radiation dose may be ascribed to the shield shape (¬ , ⌐) used in this study, which can only shield the radiation, instead of using a shield shape that can perfectly enclose the breast.

Third, among the adjacent organs, the heart was found to be exposed to a lower radiation dose than the lungs, presumably due to its deep anatomical position.

Moreover, analyses of the shielding-dependent absorbed dose to adjacent organs revealed that shielding was associated with decrease in dose to the lung on the shielded (contralateral) side and the heart; however, an increase in the dose to the ipsilateral lung was observed. This is attributable to the effects of the shield shape (¬ , ⌐), which contributes to decreasing the dose to the organs located interiorly to the shield while enhancing the dose to the organs located exteriorly to the shield as a result of radiation dose.

Finally, according to Sechopoulos *et al.* [24], long-term dose was evaluated as the relative organ dose value. When compared with the values presented in this study, the results were calculated as 0.009 in the photographed lung, 0.006 in the contralateral lung, and 0.003 in the heart, which are similar to the results obtained in the previous study.

CONCLUSION

The absorbed dose to the mammary gland in mammography is normally 2 mGy or lower. However, both breasts basically undergo series imaging and likely undergo additional mammographic exams whenever considered necessary. As a method to reduce the overall exposure dose, shielding the contralateral breast may contribute to substantially reducing the patient dose, which was investigated in this study.

The materials and shape of the shield designed in this study were chosen under the criteria of simple and practical application in clinical settings. Using a shield during screening mammography would alleviate concerns about the mammography-induced risk of breast cancer and secondary effects.

***Conflicts of interest*:** *Declared none.*

REFERENCES

1. Tromans C, Chan A, Highnam R, Wllington NZ (2014) Comparing personalized mean glandular dose estimates between X-ray system over time in mammography. *European Society of Radiology,* 1–24.
2. Duffy SW, Chen THH, Smith RA, Yen AMF, Tabar L (2013) Real and artificial controversies in breast cancer screening. *Breast Cancer Manage,* ***2(6)****: 519–528*.
3. Hur HK, Park SM, Kim GY (2005) Risk factors and early screening behavior for breast cancer in rural women. *Korean J Women Health Nurs,* ***11(1)****: 46–52*.
4. Nam SJ (2009) Screening and diagnosis for breast cancers. *J. Korean Med Assoc*, ***51(10):*** *946–951.*
5. Suh M, Choi KS, Lee YY, Jun JK (2013) Trends in cancer screening rates among Korean men and women: Results from the Korean National Cancer Screening Survey 2004-2012. *Cancer Res Treat,* ***45****: 86–94*.
6. Vinnicombe S, Pinto Pereira SM, McCormack VA, Shiel S, Perry N, Dos Santos Silva IM (2009) Full-field digital versus screen-film mammography: comparison within the UK breast screening program and systematic review of published data. *Radiology*, **251:** 347–358.

7. Tomal A, Poletti ME, Caldas LVE (2010) Evaluation of subject contrast and normalized average glandular dose by semi-analytical models. *Appl Radiat Isot,* ***68****: 755–759*.
8. Choi SY, Ko SJ, Kang SS (2013) Denoising of digital mammography images using wavelet transform. *J. Korean Soc. Radiology,* ***7(3)****: 181–189*.
9. Dance DR, Skinner CL, Young KC, Beckett JR, Kotre CJ (2000) Additional factors for the estimation of mean glandular breast dose using the UK mammography dosimetry protocol. *Phys Med Biol,* ***45(11)****: 3225–3240*.
10. Bouzsrjomehri F, Mostaar A, Ghasemi A, Eharmposh MH, Khosravi H (2006) The study of mean glandular dose in mammogarphy in yazd and the factors affection it. *Int J Radiat Res,* ***4****: 29–35*.
11. Sookpeng Sand Ketted P (2006) Mean glandular dose from routine mammography. *Naresuan University Journal,* ***14****: 19–26*.
12. Park HS, Kim HJ, Lee LC, Cho HM, Yu AR (2009) Standardization of the method of measuring average glandular dose (AGD) and evaluation of the breast composition and thickness for AGD. *J Korean Soc of Med Physics,* ***20(1)****: 21–29*.
13. Lee JS (2014) Dose evaluation using mathematical simulation of radiation exposure body in mammography system. *J Korean Soc Radiol,* ***8(4)****: 21–29*.
14. Lee SH, Lee JS, Han SH (2012) A study on absorbed dose in the breast tissue using Geant4 simulation for mammography. *J Radiol Sc & Tech,* ***35(4)****: 345–352*.
15. Yun YP (2008) Guidelines for patient dose recommendations in mammographic X-ray. Korean Food & Drug Administration.
16. Han EY, Bolch WE, Eckerman KF (2006) Revision to the ORNL series of adult and pediatric computational phantoms for use with the MIRD schema. *Health Phys,* ***90****: 337–356*.
17. Valentin J (2002) Basic anatomical and physiological data for use in radiological protection reference values. International Commission on Radiological Protection, *Annals of the ICRP, Publication 89*.
18. White DR, Griffith RV, Wilson IJ (1992) Photon, electron, proton and neutron interaction data for body tissues. *Journal of the ICRU, Report 46*.
19. White DR, Booz J, Griffith RV, Spokas JJ, Wilson IJ (1989) Tissue substitutes in radiation dosimetry and measurement. *Journal of the ICRU, Report 44*.
20. Choi TJ, Oh YK, Kim JH (2010) Development of lead-free shielding for radiation protection in medical radiology. *J Korean Soc of Med Physics*, ***21(2)****: 232–237*.
21. Mowlavi AA (2005) X-ray spectra calculation for different target-filter of mammograms using MCNP code. *Int J Radiat Res,* ***3(3):*** *129–133*.
22. Jang SY, Oh WK, Park JB, Jin KH (2013) The energy spectrum and phantom image quality according to mammography target-filter combination. *J Korea Soc of Radiology*, ***7 (1)****: 51–55*.
23. Paixão L, Oliveira BB, Viloria C, de Oliveira MA, Teixeira MHA, do Socorro Nogueira M (2015) Monte Carlo derivation of filtered tungsten anode X-ray spectra for dose computation in digital mammography. *Radiol Bras,* ***48(6)****: 363–367*.
24. Sechopoulos I, Suryanarayanan S, Vedantham S, D'Orsi CJ, Karellas A (2008) Radiation dose to organs and tissues from mammography: Monte Carlo and phantom study[1]. *Radiology,* ***246(2)****: 434–443*.